A dynamic system approach to spiking second order memristor networks

This article has been accepted for publication in IEEE Transactions on Circuits and Systems--I: Regular Papers. This is the author's version which has not been fully edited and content may change prior to final publication. Citation information: DOI 10.1109/TCSI.2021.3137713

A Dynamic System Approach to Spiking Second Order Memristor Networks

Francesco Marrone, *Student Member, IEEE,*, Gianluca Zoppo, Fernando Corinto, *Senior Member, IEEE,* and Marco Gilli, *Fellow, IEEE*

***Abstract*—Second order memristors are two terminal devices that present a conductance depending on two orders of variables, namely the geometric parameters and the internal temperature. They have shown to be able to mimic some specific features of neuron synapses, specifically Spike-Timing-Dependent-Plasticity (STDP), and consequently to be good candidates for neuromorphic computing. In particular, memristor crossbar structures appear to be suitable for implementing locally competitive algorithms and for tackling classification problems by exploiting temporal learning techniques. On the other hand, neuromorphic studies and experiments have revealed the existence of different kinds of plasticity and have shown the effect of calcium concentration on synaptic changes. Computational studies have investigated the behavior of spiking networks in the context of supervised, unsupervised, and reinforcement learning. In this paper, we first derive a simplified, almost analytical, model of a second-order memristor, only involving two variables, the mem-conductance, and the temperature, directly attributable to the synaptic efficacy and to the calcium concentration. Then we study in detail the response of a single memristive synapse to the most relevant plasticity models, including cycles of spike pairs, triplets, and quadruplets at different frequencies. Finally, we accurately characterize memristor spiking networks as discrete nonlinear dynamic systems, with mem-conductances as state variables and pre and postsynaptic spikes as inputs and outputs, respectively. The result shows that the model developed in this manuscript can explain and accurately reproduce a significant portion of observed synaptic behaviors, including those not captured by classical spike pair-based STDP models. Furthermore, under such an approach, the global dynamic behavior of memristor networks and the related learning mechanisms can be deeply analyzed by employing advanced nonlinear dynamic techniques.**

***Index Terms*—Memristor, Spiking Neural Networks, STDP, Neuromorphic Computing.**

I. Introduction

MEMRISTORS and memristive systems were theoretically conceived by L. O. Chua [1], [2] and firstly realized as thin-film electrical elements, based on Titanium Oxide, [3]. They have been widely exploited in analog and digital systems for a broad scope of applications, including amplifiers, filters, oscillators, logic gates and pseudo-random number generators [4], [5], [6]. In terms of voltage-current characteristic a two terminal memristor device is described by a mem-conductance, which may depend on a set of first and second order state variables, linked to the internal geometric parameters and to the internal temperature respectively. Due to their intrinsic properties, memristors have found to be suitable to emulate some synaptic functions and consequently to be attractive candidates for neuromorphic computing [7], [8], [9], [10]. In particular second order memristors have shown to be able to mimic a crucial synaptic feature, specifically Spike-Timing-Dependent-Plasticity (STDP) [8] and memristor crossbar structures appear to be qualified to implement locally competitive algorithms (LCA) and to tackle classification problems, by exploiting STDP rules and temporal learning techniques [15], [14]. In the last two decades many studies and experiments in neuroscience have shown the effect of spike-timing on synaptic efficacy. Early experiments [16], [17] have revealed that a sequence of pairs of presynaptic and postsynaptic spikes gives rise to potentiation, whereas depression is observed if presynaptic spikes follow postsynaptic ones. As a consequence synaptic plasticity has been characterized by the time difference between pair of spikes and many STDP models have been investigated, both from the biophysical and the computational point of view [18], [19], [20]. Further experiments have shown that spike pairs are not able to explain more complex protocols, for example synaptic changes when the repetition frequency increases [18]. In order to characterize such a large variety of synaptic behavior, new phenomenological models were introduced, based on elementary blocks composed of three/four spikes (triplets/quadruplets) [21], [22], [23], [24]. It was found that classical STDP models, based on spike pairs are not sufficient to capture synaptic changes generated by spike triplets and quadruplets. [25].

A field of investigation, which is of specific interest for designing neuromorphic electric circuits, concerns the biophysical dynamic models of synaptic plasticity. In particular many stimulation protocols have outlined that calcium concentration dynamics plays a crucial role for inducing potentiation and depression. In [26] synaptic changes are described by means of a second order system of ODEs, with synaptic efficacy and calcium concentration as state variables and pre/post synaptic spike trains as inputs (see eq. 1 of [26] and the SI Appendix of [26]). Through this simple model a large variety of STDP curves can be reproduced, for different spike patterns, including pairs, triplets and quadruplets, and the effect of the frequency on the synaptic plasticity is accurately predicted.

Second order memristors are described as mathematical models whose internal state depends on two state variables. The advantage of using higher-order memristive devices lies in their multiple state variables that can model the operation per-

F. Marrone, G. Zoppo, F. Corinto, and M. Gilli are with the Department of Electronics and Telecommunications, Politecnico di Torino, Torino, Italy, (e–mails: francesco.marrone@polito.it, gianluca.zoppo@polito.it, fernando.corinto@polito.it, marco.gilli@polito.it).

This work was supported by the Ministero dell'Istruzione, dell'Universitá e della Ricerca (MIUR) under Contract 2017LSCR4K-003.

formed by biological synapses. For example, [8] presents some surprising similarities with respect to the biophysical model presented in [26], by assuming that the role of the synaptic efficacy and of the calcium concentration is played by the mem-conductance and by the memristor internal temperature respectively. This fact has been exploited in [8] to show that a second-order memristor is capable of reproducing some crucial features of synaptic plasticity, in particular potentiation and depression in presence of pre/post (post/pre) synaptic spikes, suitably modeled as sequence of heating and programming pulses. The capability of second order memristor to model synaptic plasticity with spike triplets and the related STDP rules were investigated in [10]. Many different models with different complexity have been proposed in the literature. However, there is an ongoing debate over which model should be adopted for the investigation of biological phenomena [11], [12], [13].

In parallel to biophysical studies, an important research topic in computational neuroscience and neuromorphic engineering has regarded spiking neural networks that are attractive systems for real-time applications, primarily if they are implemented in hardware platforms, like memristor crossbar networks [15], [27]. Spiking networks have been shown to exhibit the same computational power of conventional artificial neuron networks (ANNs) [28]. Starting from the relation between spiking and Hebbian learning [27], they have been investigated in the context of supervised, unsupervised and reinforcement learning [29], [30]. However, they have not reached the same accuracy as ANNs, mainly because of the lack of adequate and efficient training algorithms.

This manuscript, which is an extension of some conference papers [31], [32], [33], presents three main results. First, we derive a simplified ODE model of a second-order memristor, based on [8], that only involves two state variables, the memcomductance, and the internal temperature, directly ascribable to the already mentioned biophysical quantities, namely the synaptic efficacy and the calcium concentration. Through this model the mem-conductance variation, due to various combinations of spike inputs, can be almost analytically computed. Second, we examine in detail the memristor behavior as a single synapse by studying the response to some relevant plasticity models, in particular cycles of spike pairs, triplets, and quadruplets at different frequencies. We show that through our approach: I) the most significant synaptic properties of second-order memristors can be easily studied and predicted; II) a significant portion of the synaptic behaviors that are not captured by classical spike pair based STDP models can be readily reproduced. Third, we accurately characterize memristor spiking networks as discrete nonlinear dynamic systems, with mem-conductances as state variables and pre and postsynaptic spikes as inputs and outputs. We explicitly derive the state equations governing the mem-conductance evolution, and we show that the network response to periodic presynaptic inputs can be readily determined by computing the system equilibrium points and discussing their stability properties. Through our approach, we are confident that the response of memristor networks to arbitrary presynaptic inputs and the underlying learning mechanisms can be effectively investigated by employing advanced nonlinear dynamic techniques.

II. Second order memristor model

We consider the second order memristor illustrated in Fig. S8b of the *SI Appendix* of [8], which exhibits a conductive region divided into three serial parts: base-conductive filament (CF), sub-CF, and depleted gap. In accordance with eqs. (S5a)-(S5e) and eqs. (S6)-(S9) of [8], the memristor is described as a two terminal circuit element, with the following relation between the voltage $\mathbf{v}(t)$ and the current $\mathbf{i}(t)$:

$$\begin{aligned}\mathbf{v}(t) &= \frac{\rho\mathcal{L}_0}{\pi r_0^2}\, I_0 \left[1+\frac{L-\mathcal{L}_0-\mathbf{g}}{\mathcal{L}_0}\left(\frac{r_0}{\mathbf{r}}\right)^2\right]\frac{\mathbf{i}(t)}{I_0} \\ &\quad + V_0 \sinh^{-1}\left[\frac{\mathbf{i}(t)}{I_0}\exp\left(\frac{\mathbf{g}}{g_m}\right)\right] \end{aligned} \tag{1}$$

where, according to Table *S1* of [8], $L = 5\,nm$ is the total layer thickness, $\rho = 2.2\,10^{-6}\,S/m$ is the resistivity of the CF regions, $r_0 = 2.5\,nm$ and $\mathcal{L}_0 = 2.5\,nm$ are the constant radius and length of the base-CF region, $\mathbf{r}$ is the modulated radius of the sub-CF region, $\mathbf{g}$ is the gap length and $I_0 = 15\,mA$, $V_0 = 0.2\,V$, $g_m = 0.2\,nm$ are parameters depending on the material.

The radius $\mathbf{r}$ and the gap length $\mathbf{g}$ are two dynamic variables, whose evolution is governed by the following system of ODEs, which strongly depend on the temperature $\mathbf{T}$ of the inner region around the filament:

$$\frac{d\,\mathbf{g}}{d\,t} = \begin{cases} -\frac{1}{2}\,\exp\left(-\frac{E_a}{k_b\mathbf{T}}\right)\,\zeta(t) & (\mathbf{v}\geq 0) \\ -\frac{1}{2}\,\exp\left(-\frac{E_a}{k_b\mathbf{T}}\right)\,\left(\frac{r_0}{\mathbf{r}}\right)^2\,\zeta(t) & (\mathbf{v}<0) \end{cases} \tag{2}$$

$$\zeta(t) = \frac{\alpha\,a^2\,f}{\mathcal{L}_0-\mathbf{g}} - 2\,a\,f\sinh\left(\frac{q\,a\,\mathbf{v}}{\mathbf{g}\,k_b\,\mathbf{T}}\right) \tag{3}$$

$$\frac{d\,\mathbf{r}}{d\,t} = \begin{cases} -\frac{1}{2}\,\exp\left(-\frac{E_a}{k_b\mathbf{T}}\right)\,\left[\frac{\beta\,a^2\,f}{\mathbf{r}-r_m}\right] & (\mathbf{v}\geq 0) \\ +\frac{1}{2}\,\exp\left(-\frac{E_a}{k_b\mathbf{T}}\right)\,\left(\frac{r_0}{\mathbf{r}}\right)^2\,\left[\frac{\beta\,a^2\,f}{\mathbf{r}-r_m}\right] & (\mathbf{v}<0) \end{cases} \tag{4}$$

In the above equations (2)-(4) , $E_a = 0.85\,eV$ represents the ion migration energy barrier, $k_b = 1.38\,10^{-23}\,J/K$ is the Boltzmann constant, $q = 1.6\,10^{-19}\,C$ is the electron charge, $f = 10^{12}\,Hz$ is the escape-attempt frequency, $a = 0.1\,nm$ is the hopping distance, and $r_m = 0.8\,nm$, $\alpha = 3\,10^4$, $\beta = 8\,10^3$ are model parameters estimated in [8].

The dynamics of the internal temperature $\mathbf{T}$ is described by the following set of two coupled ODEs, which are expressed in term of the bulk temperature $\mathbf{T_b}$ of the outer region:

$$C_{p1}\,\frac{d\,\mathbf{T}}{d\,t} = \mathbf{v}(t)\,\mathbf{i}(t) - k_{th1}\,(\mathbf{T}-\mathbf{T_b}) \tag{5}$$

$$C_{p2}\,\frac{d\,\mathbf{T}_b}{d\,t} = \mathbf{v}(t)\,\mathbf{i}(t) - k_{th2}\,(\mathbf{T}_b-300) \tag{6}$$

where $Cp1$, C_{p2} and k_{th1}, k_{th2} are fitting parameters denoting the effective heat capacitances and the effective thermal conductances respectively.

In accordance with the parameters used in the spice simulation reported in the *SI Appendix* of [8] we have assumed

This article has been accepted for publication in IEEE Transactions on Circuits and Systems--I: Regular Papers. This is the author's version which has not been fully edited and content may change prior to final publication. Citation information: DOI 10.1109/TCSI.2021.3137713

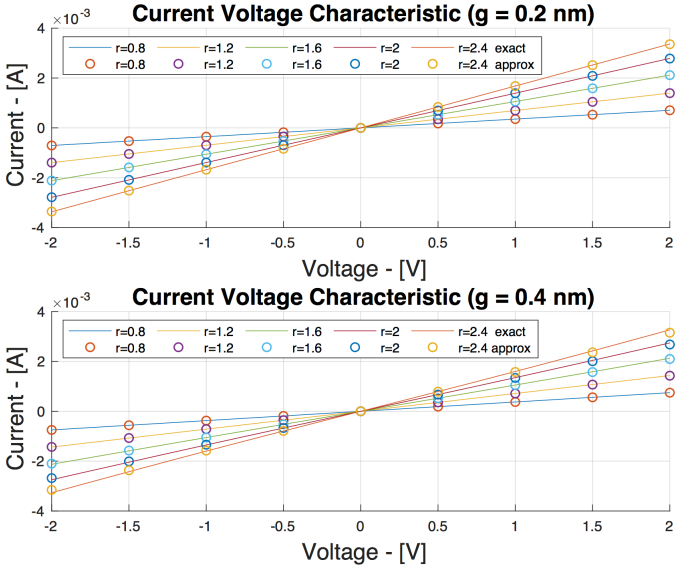

Figure 1: Current-voltage characteristic, for different values of the radius $\mathbf{r}$ (expressed in nm), and of the gap length ($\mathbf{g} = 0.2\,nm$, and $\mathbf{g} = 0.4\,nm$). Solid lines represent the exact characteristic, obtained by numerically inverting the $\mathbf{v}$-$\mathbf{i}$ relation (1); the current values derived from the approximate expression of the mem-conductance given in (9) are represented as circles.

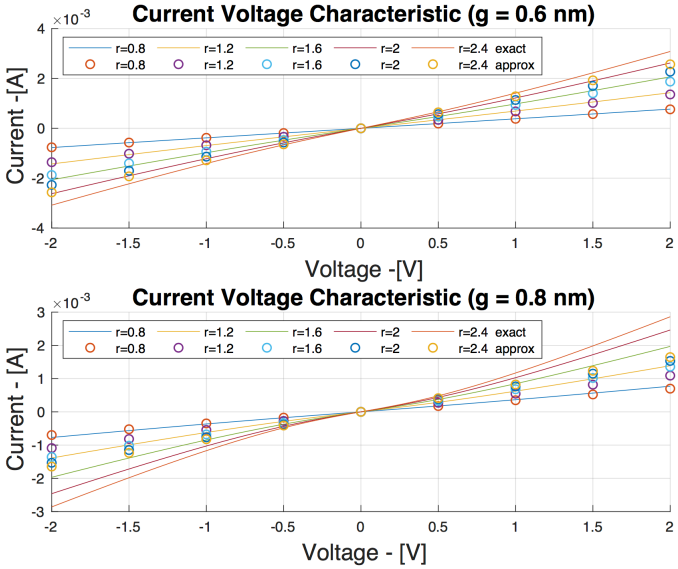

Figure 2: Current-voltage characteristic, for different values of the radius $\mathbf{r}$ (expressed in nm), and of the length gap ($\mathbf{g} = 0.6\,nm$, and $\mathbf{g} = 0.8\,nm$). Solid lines represent the exact characteristic, obtained by numerically inverting the $\mathbf{v}$-$\mathbf{i}$ relation (1); the current values derived from the approximate expression of the mem-conductance given in (9) are represented by circles.

$k_{th1} = 2.8\,10^{-5}\,JK^{-1}s^{-1}$, $k_{th2} = 5.4/5.5\,10^{-5}\,JK^{-1}s^{-1}$ and the following values for the temperature and the bulk temperature time constants τ_T and τ_b:

$$\tau_T = \frac{1}{\lambda_T} = \frac{C_{p1}}{k_{th1}} \approx 0.325\,10^{-9}\,s \quad (7)$$

$$\tau_b = \frac{1}{\lambda_b} = \frac{C_{p2}}{k_{th2}} = \frac{1}{5.4\,10^6} \approx 0.185\,10^{-6}\,s \quad (8)$$

The internal temperature time constant τ_T turns out to be of some order of magnitude smaller than the bulk temperature time constant τ_b. This latter property, which also holds if the fitting parameters are differently estimated, is essential for explaining the role played by the temperature in second order memristors.

III. Comparison between the memristor model and the calcium based biophysical model

The second order model derived in [8] and briefly described above is expressed by the algebraic equation (1) , that cannot be inverted in a closed form, and by a set of four nonlinear coupled ODEs (2)-(4), (5)-(6). A first significant difference with respect to the calcium based model presented in [26] is that a direct expression of the time-evolution of the mem-conductance, representing a synaptic efficacy variable, is not directly available, as in eq. (1) of [26]. A second major difference regards the roles played by the internal temperature $\mathbf{T}$ and the calcium concentration in equations (2)-(4) and in eq. (1) of [26] respectively.

In this section, to deeply understand and exploit memristors neuromorphic features, we derive a simplified model of second-order memristors, involving only two dynamic variables, the mem-conductance, and the temperature, which are directly ascribable to the synaptic efficacy and to the calcium concentration of [26].

By exploiting (1) the direct relationship between the current $\mathbf{i}(t)$ and the voltage $\mathbf{v}(t)$ can be numerically computed and the mem-conductance turns out to be a function of the voltage $\mathbf{v}(t)$, of the radius $\mathbf{r}$ and of the gap length $\mathbf{g}$. An explicit form of the mem-conductance can be derived in two ways. The first one is to exploit a first order approximation of the $\sinh^{-1}$ function, valid for $\left|\frac{\mathbf{i}(t)}{I_0}\exp\left(\frac{\mathbf{g}}{g_m}\right)\right| < 1$, which gives rise to the following expression:

$$\tilde{\mathbf{G}}\left(\mathbf{g},\mathbf{r}\right) = \frac{1}{\frac{\rho\mathcal{L}_0}{\pi r_0^2}\left[1+\frac{L-\mathcal{L}_0-\mathbf{g}}{\mathcal{L}_0}\left(\frac{r_0}{\mathbf{r}}\right)^2\right] + \frac{V_0}{I_0}\exp\left(\frac{\mathbf{g}}{g_m}\right)} \quad (9)$$

The accuracy of the above expression can be checked by reporting in a graph the exact and the approximate relationship between the current $\mathbf{i}(t)$ and the voltage $\mathbf{v}(t)$ for different values of $\mathbf{g}$ and $\mathbf{r}$, as shown in Figs. 1-2. As expected, it is observed that for a given radius $\mathbf{r}$, a reasonable range of input voltages, and relatively small values of the gap length $\mathbf{g}$, the $\mathbf{i}$-$\mathbf{v}$ characteristic is almost linear and accurately represented by the approximate expression (9). Some numerical inaccuracies occur for larger values of $\mathbf{g}$. However, by computing the stationary points of equation (2), governing the gap length evolution, it can be shown that large values of $\mathbf{g}$ are not reached for actual temperature and voltage ranges.

The second way to approximate the $\mathbf{i}$-$\mathbf{v}$ characteristic is to observe that the mem-conductance presents a weak dependence on the gap length $\mathbf{g}$, as shown in Figs. 3-4. It is noticed that for voltage higher than 1 V the mem-conductance is almost constant with respect to the gap length and it substantially only depends on the radius $\mathbf{r}$. For smaller voltages

This article has been accepted for publication in IEEE Transactions on Circuits and Systems--I: Regular Papers. This is the author's version which has not been fully edited and content may change prior to final publication. Citation information: DOI 10.1109/TCSI.2021.3137713

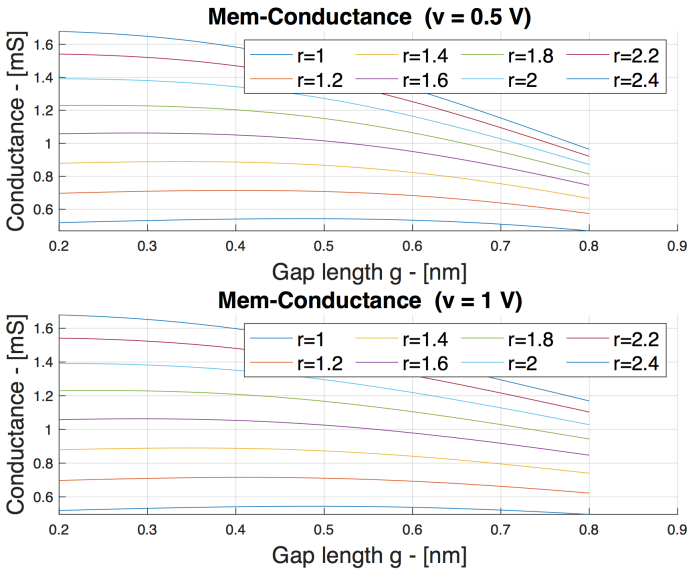

Figure 3: Mem-conductance, as a function of the gap length $\mathbf{g}$, for different values of the radius $\mathbf{r}$ (expressed in nm), and different voltages ($\mathbf{v} = 0.5\,V$, and $\mathbf{v} = 1\,V$).

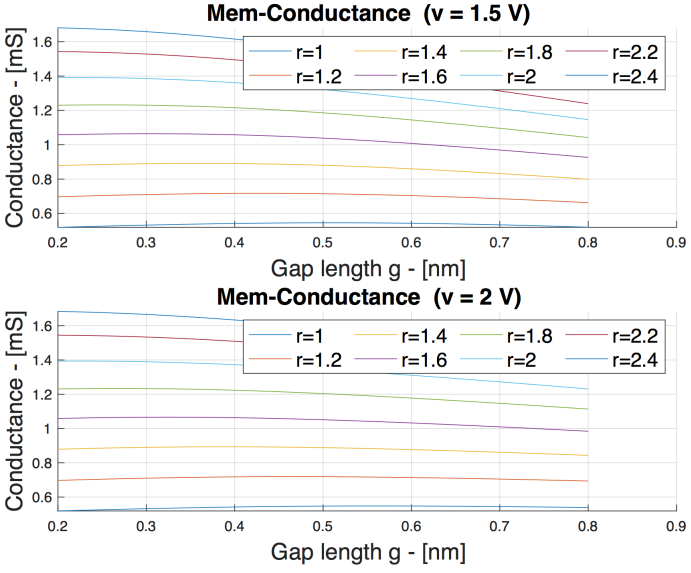

Figure 4: Mem-conductance, as a function of the gap length $\mathbf{g}$, for different values of the radius $\mathbf{r}$ (expressed in nm), and different voltages ($\mathbf{v} = 1.5\,V$, and $\mathbf{v} = 2\,V$).

it is easily shown, in accordance with (2), that only a limited extension of the gap length is admissible, e.g. $\mathbf{g} < 0.4$ nm, and consequently the mem-conductance can still be considered mainly dependent on the radius $\mathbf{r}$.

It is worth noting that, despite such a strong approximation, simulations results show that the resulting expression is reasonably accurate and able to explain all the relevant plasticity properties of second order memristors (see Appendix A where the mem-conductance approximation is justified in detail and it is shown that it holds for any admissible activation energy E_a).

From (1), by only considering the base-CF and sub-CF regions and by noting that $\mathcal{L}_0 = 0.5\,L$, it is obtained:

$$\hat{\mathbf{G}}(\mathbf{r}) = \frac{1}{R_s\left[1+\left(\frac{r_0}{\mathbf{r}}\right)^2\right]}, \qquad \left(R_s = \frac{\rho \mathcal{L}_0}{\pi r_0^2}\right) \tag{10}$$

and consequently the variable $\mathbf{r}$ can be expressed as a function of the approximate conductance $\hat{\mathbf{G}}$:

$$\mathbf{r} = r_0\sqrt{\frac{R_s\hat{\mathbf{G}}}{1-R_s\hat{\mathbf{G}}}} \tag{11}$$

The following expression of the time derivative of the mem-conductance $\hat{\mathbf{G}}$ is readily derived from (10) and (4):

$$\begin{aligned}\frac{1}{\hat{\mathbf{G}}}\frac{d\hat{\mathbf{G}}}{dt} &= \frac{1}{\hat{\mathbf{G}}}\frac{d\hat{\mathbf{G}}}{d\mathbf{r}}\frac{d\mathbf{r}}{dt} = 2\,\frac{1}{\mathbf{r}}\,(1-R_s\hat{\mathbf{G}})\,\frac{d\mathbf{r}}{dt} \\ &= \exp\left(-\frac{E_a}{k_b\mathbf{T}}\right)\,\eta(\hat{\mathbf{G}})\end{aligned} \tag{12}$$

$$\eta(\hat{\mathbf{G}}) = \frac{\sqrt{\frac{(1-R_s\hat{\mathbf{G}})^3}{R_s\hat{\mathbf{G}}}}}{\sqrt{\frac{R_s\hat{\mathbf{G}}}{1-R_s\hat{\mathbf{G}}}}-\frac{r_m}{r_0}}\left(\frac{a}{r_0}\right)^2\beta f\begin{cases}-1 & (\mathbf{v}\geq 0)\\ \frac{1-R_s\hat{\mathbf{G}}}{R_s\hat{\mathbf{G}}} & (\mathbf{v}<0)\end{cases} \tag{13}$$

As expected, the above expression can be directly compared with equation (1) of [26] since it only depends on $\hat{\mathbf{G}}$ and $\mathbf{T}$, which play the role of the synaptic efficacy and of the calcium concentration.

As far as temperature dynamic equations (5)-(6) are concerned, we exploit the fact that spikes can be modeled by constant input voltages, applied for short time periods. Since the conductance dynamics is significantly slower than the temperature dynamics, governed by time constants (7)-(8), we can assume that for the time intervals of interest (around $20\,ns$ and $1\,\mu s$ for programming and heating voltages, according to [8]) the conductance exhibits small variation with respect to the temperature and can be considered almost constant. By denoting with $\overline{\mathbf{G}}$ the value of the conductance and by $\mathbf{V}$ the constant voltage, the following expressions hold for the temperatures $\mathbf{T}$ and $\mathbf{T}_b$ in a generic interval $[t_0,\,t]$:

$$\begin{aligned}\mathbf{T_b}(t) &= \exp[-\lambda_b(t-t_0)]\;(T_b(t_0)-T_b^\infty)+T_b^\infty \\ T_b^\infty &= 300+\frac{1}{k_{th2}}\overline{\mathbf{G}}\mathbf{V}^2\end{aligned} \tag{14}$$

$$\begin{aligned}\mathbf{T}(t) &= \exp[-\lambda_T\,(t-t_0)]\left(T(t_0)-\frac{1}{k_{th1}}\overline{\mathbf{G}}\mathbf{V}^2-T_b^\infty\right) \\ &+ \frac{1}{k_{th1}}\overline{\mathbf{G}}\mathbf{V}^2+T_b^\infty \\ &+ \left\{\frac{\lambda_T}{\lambda_T-\lambda_b}\,\{\exp[-\lambda_b(t-t_0)]-\exp[-\lambda_T(t-t_0)]\}\right\} \\ &\cdot\{T_b(t_0)-T_b^\infty\}\end{aligned} \tag{15}$$

This article has been accepted for publication in IEEE Transactions on Circuits and Systems--I: Regular Papers. This is the author's version which has not been fully edited and content may change prior to final publication. Citation information: DOI 10.1109/TCSI.2021.3137713

By taking into account that, according to (7)-(8), $\lambda_T >> \lambda_b$ and that for $t - t_0$ of the order of $10 - 20\,ns$ the term $\exp[-\lambda_T\,(t - t_0)]$ is almost null, the following simplified approximated expression of the internal temperature $\mathbf{T}(t)$ is readily obtained:

$$\begin{aligned}\mathbf{T}(t) &\approx exp[-\lambda_b(t-t_0)]\;(T_b(t_0) - T_b^{\infty}) + T_b^{\infty} + \frac{1}{k_{th1}}\,\overline{\mathbf{G}}\mathbf{V}^2 \\ &\approx \mathbf{T_b}(t) + \frac{1}{k_{th1}}\overline{\mathbf{G}}\,\mathbf{V}^2 \end{aligned} \tag{16}$$

In accordance with [8], a typical input to the memristor is a pre/postsynaptic spike, composed by the sequence of a programming and a heating pulse of duration t_s and t_H, respectively. This introduces some additional complexity with respect to the standard STDP models where a single pulse represents the spikes: in particular, the programming pulse of the second post/pre synaptic spike may occur either before or after the end of the heating pulse of the first pre/post synaptic pulse. These two cases are shown in Fig. 5 for a pre/post spike pair, a similar representation holding for post/pre pair. In general we denote with γt_H the time shift between the beginning of the programming pulse of the second spike and the beginning of the heating pulse of the first spike; the parameter γ turns out to be greater than 1 if the programming pulse occurs after the end of the heating pulse and less than 1 otherwise.

By slightly elaborating expression (16), a very accurate analytic expression of the internal temperature $\mathbf{T}(\gamma)$ associated to the programming pulse, can be derived:

$$\mathbf{T}(\gamma) \approx 300 + \hat{\mathbf{G}}\left\{\frac{V_P^2}{k_{th1}} + \frac{V_P^2}{k_{th2}}\left[1 - \exp\left(-\frac{t_s}{\tau_b}\right)\right] + \Gamma\,\frac{V_H^2}{k_{th2}}\right\}$$

$$\Gamma = \begin{cases} \exp\left(-\frac{t_s}{\tau_b}\right)\left[1 - \exp\left(-\frac{\gamma t_H}{\tau_b}\right)\right] & \gamma < 1 \\ \exp\left(-\frac{t_s + (\gamma-1)t_H}{\tau_b}\right)\left[1 - \exp\left(-\frac{t_H}{\tau_b}\right)\right] & \gamma \geq 1 \end{cases} \tag{17}$$

where V_H and V_P denote the heating and programming pulse magnitude, $\hat{\mathbf{G}}$ denotes the approximate conductance (which is assumed to present slow variations with respect to the Temperature), k_{th1} and k_{th2} denote the effective thermal conductances of the internal and bulk temperature respectively, defined above and τ_b is the bulk temperature time constant.

The simplified model developed above involves only two equations, (12) and (17), and two variables, the mem-conductance $\hat{\mathbf{G}}$ and the internal temperature $\mathbf{T}$, which are directly attributable to the two fundamental quantities, synaptic efficacy and calcium concentration, used in biophysical models for reproducing a large variety of STDP curves [26].

In addition, it is worth noting that, a part from the memristor geometrical (r_0, r_m) and physical parameters (R_s, a, β , f, k_{th1}, k_{th2}), the two equations and hence the entire model only depends on five quantities: the magnitude of the heating and programming pulsed V_H and V_P, the ratios between the two pulses duration and the bulk temperature time-constant $\frac{t_s}{\tau_b}$ and $\frac{t_H}{\tau_b}$, and the parameter γ describing the shift between each spike pair.

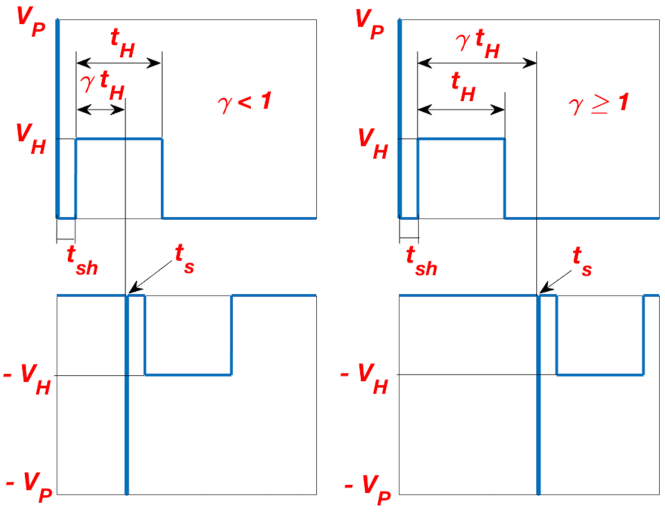

Figure 5: Input voltage corresponding to a pre/post spike pair. Each spike is represented by the sequence of a programming pulse of duration t_s and a heating pulse of duration t_H, whereas t_{sh} denotes the time shift between the programming and the heating pulse. Left part: the programming pulse of the postsynaptic spike occurs before the end of the heating pulse of the first presynaptic pulse. Right part: the programming pulse of the postsynaptic spike occurs after the end of the heating pulse of the presynaptic pulse. The time interval between two spikes is denoted by $\Delta_t = (\gamma - 1)t_H$, with γ greater than 1 in the first case and less than 1 in the second one.

IV. Memristor response to spike pairs, triplets and quadruplets

The analytic approach developed above is an effective tool for analyzing and deeply investigating synaptic properties of single second order memristors and consequently neuromorphic properties of large memristor networks.

As a first step, by substituting the expression (17) into (12) the STDP function corresponding to the mem-conductance variation, generated by a pre/post (post/pre) spike pair can be easily derived, as a function of the time interval which separates two subsequent spikes. We assume that the programming pulse of the second spike occurs after the end of the heating pulse of the first spike, i.e. $\gamma \geq 1$, and we denote such a time shift by $\Delta_t = (\gamma - 1)t_H$. Figs. 6-7 show the mem-conductance variation, due to a single pre/post (post/pre) spike pair. As expected, potentiation is observed for pre/post pairs (where Δ_t is assumed conventionally positive) whereas depression occurs for post/pre pairs (where Δ_t is assumed conventionally negative). It is worth noting that a special feature of second order memristor synapses is that the normalized variation of the mem-conductance depends on the initial value of the conductance, because the internal Temperature $\mathbf{T}$ depends on the current value of $\hat{\mathbf{G}}$ (see eq. (17)).

As already mentioned spike pairs represent a useful neuromorphic paradigm, but are not able to explain more complex protocols, like the effect of the repetition frequency on synaptic changes [18]. Such complex protocols, including experiments involving triplets and quadruplets, can be studied and readily reproduced by simply exploiting eqs. (12) and (17).

This article has been accepted for publication in IEEE Transactions on Circuits and Systems–I: Regular Papers. This is the author's version which has not been fully edited and content may change prior to final publication. Citation information: DOI 10.1109/TCSI.2021.3137713

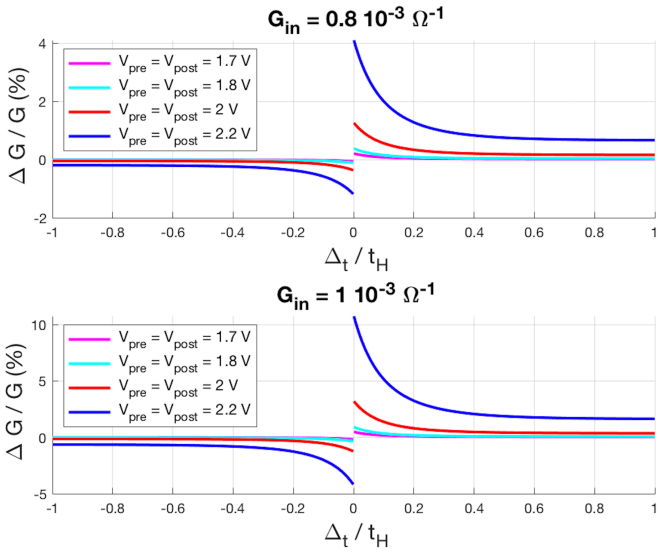

Figure 6: STDP function corresponding to the mem-conductance variation, generated by a pre/post (post/pre) spike pair, as a function of the time interval $\frac{\Delta_t}{t_H}$, which separates two subsequent spikes. It is assumed $V_H = 0.8$ V, $\frac{t_H}{\tau_b} = 5.4$, and $\frac{t_s}{\tau_b} = 0.108$; G_{in} denote the initial value of the mem-conductance.

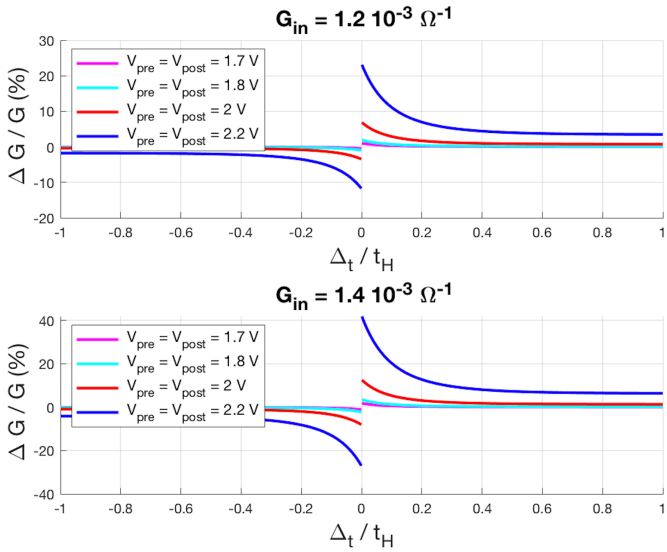

Figure 7: STDP function corresponding to the mem-conductance variation, generated by a pre/post (post/pre) spike pair, as a function of the time interval $\frac{\Delta_t}{t_H}$, which separates two subsequent spikes. It is assumed $V_H = 0.8$ V, $\frac{t_H}{\tau_b} = 5.4$, and $\frac{t_s}{\tau_b} = 0.108$; G_{in} denote the initial value of the mem-conductance.

Following the approach presented in [26] and with reference to experiments from hippocampal cultures, we examine and compare the response to spike pairs and to different configurations of spike triplets and quadruplets. A first set of results is reported in Figs. 8-9-10 which show the mem-conductance change as a function of the spike interval Δ_t, for 30 cycles of pre-post pairs, post-pre-post triplets and post-pre-pre-post quadruplets at different frequencies. The following considerations hold: 1) in all cases we observe long term potentiation (LTP) and for spike triplets the conductance saturates to the maximum acceptable value, corresponding to $\hat{\mathbf{G}} = \frac{1}{2R_s}$ in (10); 2) as expected, in case of spike pairs the potentiation decreases as the repetition frequency increases (i.e. as the time interval t_f between two pairs decreases), which is not in agreement with most experimental protocols and represent a major drawback of classical STDP models [25]; 3) in order to observe a correct frequency response, spike triplets and/or quadruplets should be exploited, as reported in [25] and [26].

A second set of results is reported in Figs. 11-12 which show the mem-conductance change as a function of the spike interval Δ_t for 30 cycles of pre-post-pre triplets and pre-post-post-pre quadruplets at different frequencies. In accordance with the results reported in [26], those configurations evoke little or no potentiation.

It is shown in Appendix B that STDP functions are not significantly affected by parameter variations and consequently the proposed model is sufficiently robust to accurately describe the actual second order memristor functionalities.

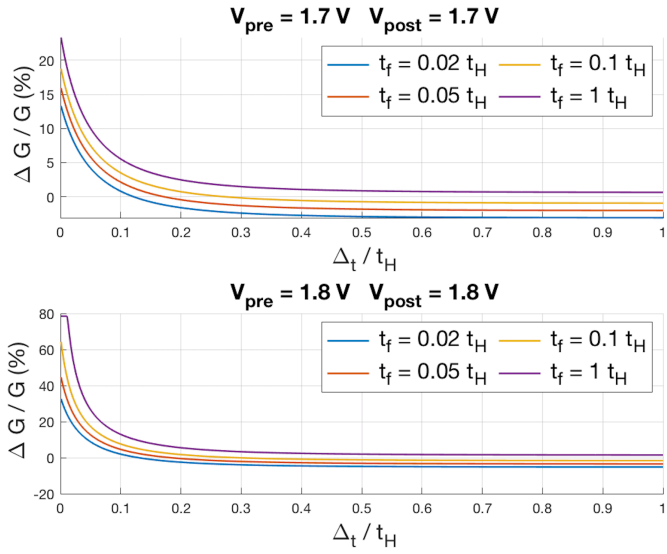

Figure 8: Mem-conductance change versus $\frac{\Delta_t}{t_H}$, for 30 cycles of pre-post pairs at different frequencies, and different programming voltages. It is assumed $V_H = 0.8$ V, $\frac{t_H}{\tau_b} = 5.4$, and $\frac{t_s}{\tau_b} = 0.108$; t_f denotes the time interval between two pairs; the initial mem-conductance is $\hat{\mathbf{G}} = 1$ mS.

V. Spiking Memristor Networks

Second order memristor networks have shown to be able to process temporal events and to classify dynamic and static data, by creating unique patterns, resulting from local potentiation and depression [14]. By using our simplified model, we will show that the pattern formation process in such networks can be studied and deeply investigated by characterizing them as discrete nonlinear dynamic systems.

This article has been accepted for publication in IEEE Transactions on Circuits and Systems--I: Regular Papers. This is the author's version which has not been fully edited and content may change prior to final publication. Citation information: DOI 10.1109/TCSI.2021.3137713

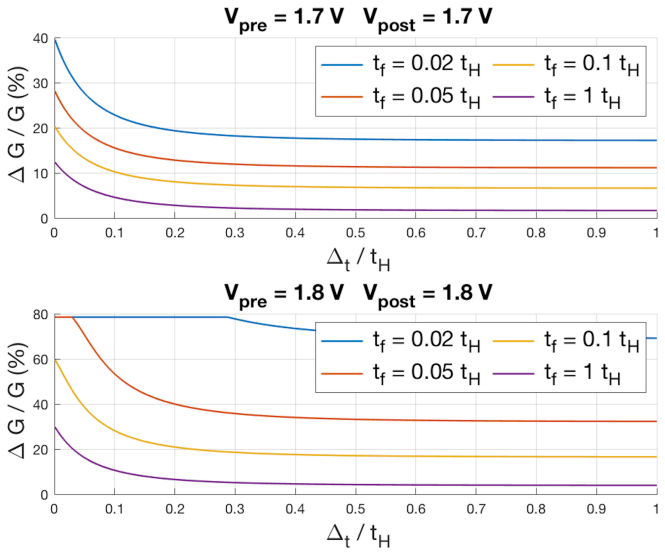

Figure 9: Mem-conductance change versus $\frac{\Delta_t}{t_H}$, for 30 cycles of post-pre-post triplets at different frequencies, and different programming voltages. It is assumed $V_H = 0.8$ V, $\frac{t_H}{\tau_b} = 5.4$, and $\frac{t_s}{\tau_b} = 0.108$; t_f denotes the time interval between two triplets; the initial mem-conductance is $\hat{\mathbf{G}} = 1$ mS.

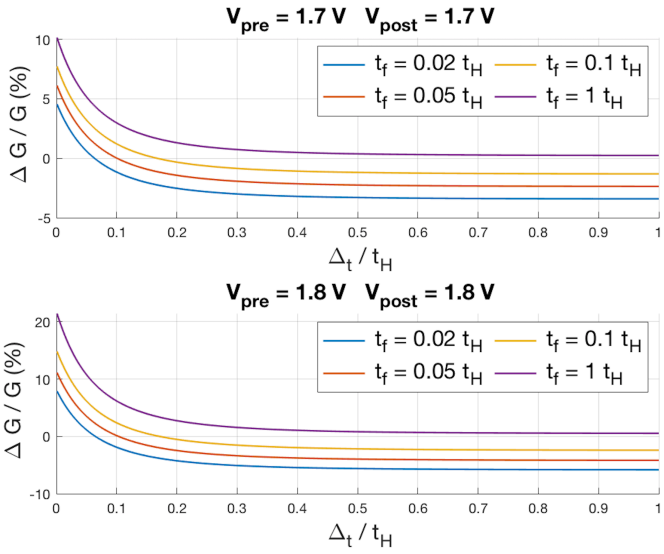

Figure 11: Mem-conductance change versus $\frac{\Delta_t}{t_H}$, for 30 cycles of pre-post-pre triplets at different frequencies, and different programming voltages. It is assumed $V_H = 0.8$ V, $\frac{t_H}{\tau_b} = 5.4$, and $\frac{t_s}{\tau_b} = 0.108$; t_f denotes the time interval between two triplets; the initial mem-conductance is $\hat{\mathbf{G}} = 1$ mS.

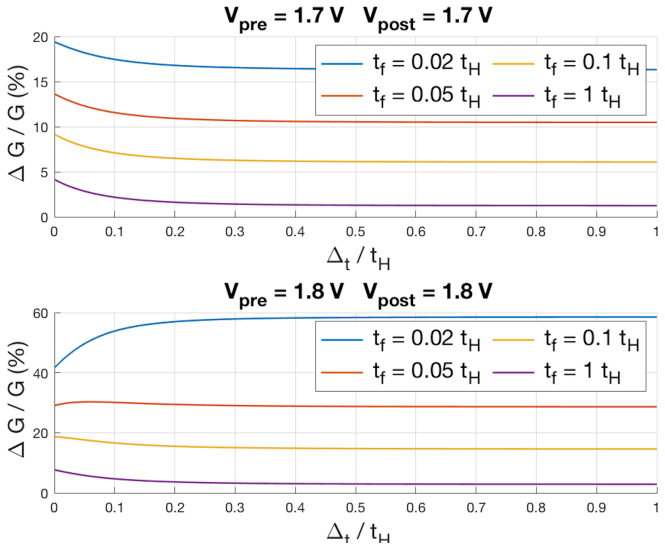

Figure 10: Mem-conductance change versus $\frac{\Delta_t}{t_H}$, for 30 cycles of post-pre-pre-post quadruplets at different frequencies, and different programming voltages. It is assumed $V_H = 0.8$ V, $\frac{t_H}{\tau_b} = 5.4$, and $\frac{t_s}{\tau_b} = 0.108$; t_f denotes the time interval between two quadruplets; the initial mem-conductance is $\hat{\mathbf{G}} = 1$ mS.

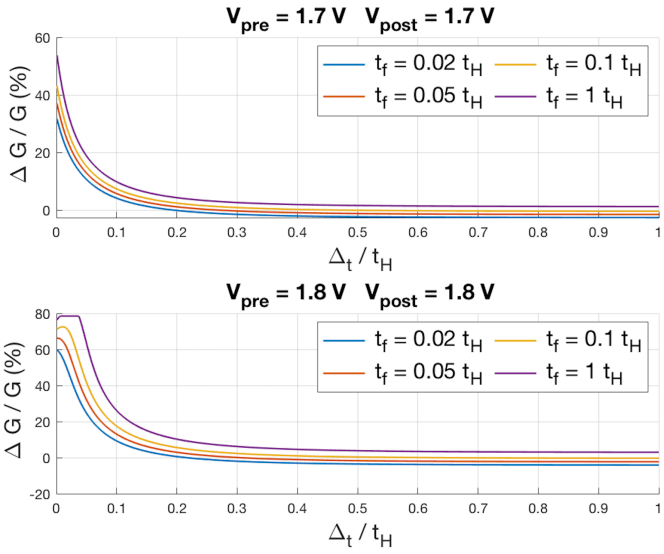

Figure 12: Mem-conductance change versus $\frac{\Delta_t}{t_H}$, for 30 cycles of pre-post-post-pre quadruplets at different frequencies, and different programming voltages. It is assumed $V_H = 0.8$ V, $\frac{t_H}{\tau_b} = 5.4$, and $\frac{t_s}{\tau_b} = 0.108$; t_f denotes the time interval between two quadruplets; the initial mem-conductance is $\hat{\mathbf{G}} = 1$ mS.

We consider a structure composed by N presynaptic neurons and M postsynaptic neurons, connected through a matrix of second-order memristors, which exhibit a conductance described by eqs. (12)-(13) and (17). The input data may be encoded through a temporal or rate code, giving rise for each neuron to a set of presynaptic spikes. As already discussed, each presynaptic/postsynaptic spike may be modeled as a positive/negative programming pulse of amplitude V_{pre}/V_{post} and duration t_s, followed by a longer negative/positive heating pulse of magnitude V_H and duration t_H. We indicate with X_j and Y_i the ensembles of all the spikes of the generic presynaptic neuron j and postsynaptic neuron i respectively:

$$\begin{aligned} X_j &= \left\{ t_{j,1}^{pre}, t_{j,2}^{pre}, \ldots, t_{j,K_j}^{pre} \right\} \\ Y_i &= \left\{ t_{i,1}^{post}, t_{i,2}^{post}, \ldots, t_{i,H_i}^{post} \right\} \end{aligned} \tag{18}$$

This article has been accepted for publication in IEEE Transactions on Circuits and Systems--I: Regular Papers. This is the author's version which has not been fully edited and content may change prior to final publication. Citation information: DOI 10.1109/TCSI.2021.3137713

where $t_{j,k}^{pre}$ $(1 \leq k \leq K_j)$ denotes the time when neuron j emits its kth presynaptic spike and $t_{i,h}^{post}$ $(1 \leq h \leq H_i)$ denotes the time when neuron i emits its hth postsynaptic spike.

We conventionally assume that all spikes occur at the beginning of the programming pulse of duration t_s and that the postsynaptic neuron voltage $u_i(t)$ is reset to zero, as soon as it exceeds a given threshold, and consequently emits a postsynaptic spike $t_{i,h}^{post}$. The voltage $u_i(t)$ turns out to be described by the following expression:

$$\begin{aligned} u_i(t) &= R \sum_{h=1}^{H_i+1} \sum_{j=1}^{N} \sum_{t_{jk}^{pre} \in (t_{i,h-1}^{post}, t_{i,h}^{post})} \hat{\mathbf{G}}_{i,j}(t_{j,k}^{pre})\, v_{j,k}^{pre}(t) \\ v_{j,k}^{pre}(t) &= V_H \left[\epsilon(t - t_{sh} - t_{j,k}^{pre}) - \epsilon(t - t_{sh} - t_H - t_{j,k}^{pre})\right] \\ &\quad + V_P \left[\epsilon(t - t_{j,k}^{pre}) - \epsilon(t - t_s - t_{j,k}^{pre})\right] \\ \epsilon(t) &= \Theta(t)\left[1 - \exp\left(-\frac{t}{\tau_m}\right)\right] \end{aligned} \tag{19}$$

where R is a resistive constant, τ_m is the postsynaptic neuron time constant, $\Theta(\cdot)$ is the Heaviside function, $[t_{i,0}^{post} t_{i,H_i+1}^{post}]$ represents the interval under consideration, $\hat{\mathbf{G}}_{i,j}(t_{j,k}^{pre})$ denotes the value of the mem-conductance at $t = t_{j,k}^{pre}$, and t_{sh} denotes the time shift between the beginning of the programming pulse and the beginning of the heating pulse, shown in Fig. (13).

By denoting the voltage threshold with u^{th} and with $\hat{\mathbf{G}}_{i,j}^{h}$ the value assumed by the time-variant mem-conductance at $t = t_{i,h}^{post}$, in correspondence of the h^{th} postsynaptic spike of neuron i, the mem-conductance dynamic evolution can accordingly be described by the following set of $N \times M$ discrete-time state equations:

$$\begin{aligned} \hat{\mathbf{G}}_{i,j}^{h+1} &= \min\left\{G_{max}, \hat{\mathbf{G}}_{i,j}^{h+1/2} + \Delta_G^{pre/post}(\hat{\mathbf{G}}_{i,j}^{h+1/2}, \gamma^{pre/post})\right\} \\ \hat{\mathbf{G}}_{i,j}^{h+1/2} &= \max\left\{G_{min}, \hat{\mathbf{G}}_{i,j}^{h} + \Delta_G^{post/pre}(\hat{\mathbf{G}}_{i,j}^{h}, \gamma^{post/pre})\right\} \end{aligned} \tag{20}$$

$$\begin{aligned} \gamma^{post/pre} &= \frac{t_{j,k_F^h}^{pre} - t_{i,h}^{post} - t_{sh}}{t_H} \\ \gamma^{pre/post} &= \frac{t_{i,h+1}^{post} - t_{j,k_L^h}^{pre} - t_{sh}}{t_H} \end{aligned} \tag{21}$$

with

$$u_i(t_{i,h}^{post}) = u^{th} \text{ and } \forall\, t \neq t_{i,h}^{post} \;\rightarrow\; u_i(t) < u^{th} \quad (1 \leq h \leq H_i) \tag{22}$$

In the above equations, k_F^h and k_L^h are the indexes of the first and of the last presynaptic spike of neuron j occurring in the time interval $[t_{i,h}^{post}, t_{i,h+1}^{post})$, $\hat{\mathbf{G}}_{i,j}^{h+1/2}$ denotes the conductance value due to the first variation $\Delta_G^{post/pre}$ determined by the post/pre pair and $\hat{\mathbf{G}}_{i,j}^{h}$ denotes the final value of the conductance due to the second variation $\Delta_G^{pre/post}$ determined by the pre/post pair. G_{max} and G_{min} represent the maximum and the minimum value, that, according to (10), each mem-conductance can reach:

$$\begin{aligned} G_{max} &= \hat{\mathbf{G}}(r_0) = \frac{1}{2\,R_s} \\ G_{min} &= \hat{\mathbf{G}}(r_m) = \frac{1}{R_s\left[1 + \left(\frac{r_0}{r_m}\right)^2\right]} \end{aligned} \tag{23}$$

The conductance variations $\Delta_G^{post/pre}(\hat{\mathbf{G}}_{i,j}^{h}, \gamma^{post/pre})$ and $\Delta_G^{pre/post}(\hat{\mathbf{G}}_{i,j}^{h+1/2}, \gamma^{pre/post})$ can be readily computed by substituting in (12)-(13) the conductance values and in (17) the appropriate values of $\gamma^{post/pre}$, $\gamma^{pre/post}$ given in (21).

The set of equations (20) - (21) - (22) together with (19) can be effectively employed to study the dynamic behavior of a memristor spiking network, with arbitrary presynaptic input spikes X_j.

VI. Network Response to Presynaptic Periodic Input Spikes

In order to show the potentiality of the method of analysis that we have developed, we consider the network response to a sequence of periodic presynaptic spikes. By employing the formalism introduced in (18), with $K_j = 1$ for all cells, the series of N presynaptic spikes can be visualized by the vector below assuming that the time shift between two subsequent spikes be constant and equal to a constant period T:

$$\mathcal{I} = \left\{t_{1,1}^{pre},\, t_{2,1}^{pre},\, \cdots,\, t_{N,1}^{pre}\right\} \quad (t_{j+1,1}^{pre} - t_{j,1}^{pre} = T,\;\; 1 \leq j \leq N-1) \tag{24}$$

Since in memristor crossbar networks, all columns are uncoupled, without losing in generality we only consider a postsynaptic neuron i. According to (19), we assume that the contribution of the programming pulses to the membrane voltage $u_i(t)$ is negligible because of their short duration. Consequently, a given threshold u^{th} triggering a postsynaptic spike may only occur in correspondence to a presynaptic neuron heating pulse. In such a case, we denote with $\alpha_j t_H$ $(\alpha_j > 0)$ the time shift between the postsynaptic spike and the beginning of the generic j^{th} heating pulse at which the threshold u^{th} is reached (see Fig. (13) for details). The following Proposition holds:

Proposition 1. *Let a network be composed of N presynaptic neurons and one postsynaptic neuron and let us assume that N is a multiple of an integer P and that the input $\mathcal{I}$, given by (24), is presented multiple times to the postsynaptic neuron. Let us consider the following set of $P+1$ equations:*

$$\begin{aligned} \Delta^{pre/post/pre}(\hat{\mathbf{G}}_p^0, \gamma_p^{post/pre}, \gamma_p^{pre/post}) &= \hat{\mathbf{G}}_p^1 - \hat{\mathbf{G}}_p^0 = 0 \\ &\quad (1 \leq p \leq P) \end{aligned} \tag{25}$$

$$\begin{aligned} \hat{\mathbf{G}}_p^1 &= \min\left\{G_{max}, \hat{\mathbf{G}}_p^{1/2} + \Delta_G^{pre/post}(\hat{\mathbf{G}}_p^{1/2}, \gamma_p^{pre/post})\right\} \\ \hat{\mathbf{G}}_p^{1/2} &= \max\left\{G_{min}, \hat{\mathbf{G}}_p^{0} + \Delta_G^{post/pre}(\hat{\mathbf{G}}_p^{0}, \gamma_p^{post/pre})\right\} \end{aligned} \tag{26}$$

$$\begin{aligned} \gamma_p^{post/pre} &= \frac{pT - \alpha\, t_H - 2t_{sh}}{t_H} \\ \gamma_p^{pre/post} &= \frac{(P-p)T + \alpha\, t_H}{t_H} \end{aligned} \tag{27}$$

This article has been accepted for publication in IEEE Transactions on Circuits and Systems--I: Regular Papers. This is the author's version which has not been fully edited and content may change prior to final publication. Citation information: DOI 10.1109/TCSI.2021.3137713

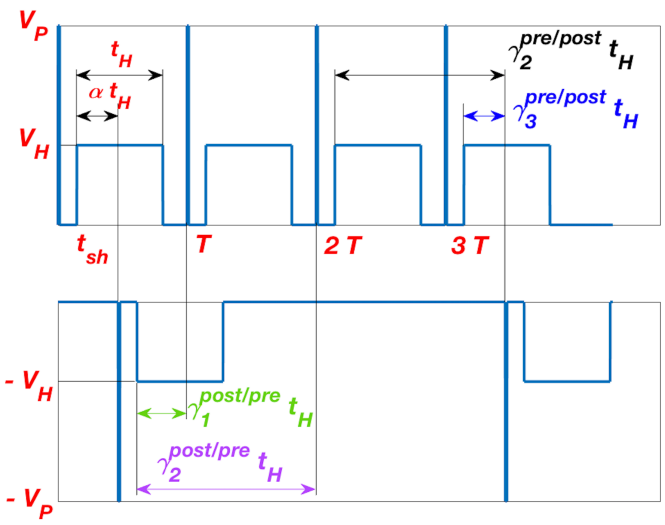

Figure 13: Example of a sequence of presynaptic input spikes of period T (upper figure), giving rise to postsynaptic output of period $3T$. Each pre/post synaptic spike is represented by a programming pulse of magnitude V_P and duration t_s, followed by a heating pulse of duration t_H; the time interval between the beginning of the programming pulse and the beginning of the heating pulse is denoted with t_{sh}. It is assumed that the postsynaptic spike occurs αt_H time units after the beginning of one presynaptic spike (with $0 \leq \alpha \leq 1$) and the following parameters, reported in (27), are shown for some mem-conductances: $\gamma_{1,2}^{post/pre}$ (related to the time shift between the beginning of the presynaptic programming pulses and the beginning of the postsynaptic heating pulse) and $\gamma_{2,3}^{pre/post}$ (related to the time shift between the beginning of the postsynaptic programming pulse and the beginning of the presynaptic heating pulses).

$$u^{th} = RV_H \left\{ \sum_{p=1}^{P-1} \hat{\mathbf{G}}_p^{1/2} \exp\left(-\frac{(P-p)T}{\tau_m}\right) \left[\exp\left(-\frac{(\alpha-1)t_H}{\tau_m}\right) - \exp\left(-\frac{\alpha t_H}{\tau_m}\right)\right] + \hat{\mathbf{G}}_P^{1/2} \left[1 - \exp\left(-\frac{\alpha t_H}{\tau_m}\right)\right] \right\} \quad (28)$$

and the following inequality:

$$RV_H \sum_{p=1}^{P-1} \hat{\mathbf{G}}_p^{1/2} \exp\left(-\frac{(P-p)T}{\tau_m}\right) \left[1 - \exp\left(-\frac{(t_H}{\tau_m}\right)\right] < u^{th} \quad (29)$$

If the inequality (29) is satisfied and there exist $\alpha > 0$ and P mem-conductances $\hat{\mathbf{G}}_p^0$, $(1 \leq p \leq P)$ satisfying the above set of $P+1$ equations (25) - (28), then the discrete time system (20) - (22) exhibits a steady state solution, which presents the following features: 1) mem-conductance patterns have a spatial periodicity of order P; 2) postsynaptic spikes occur with a temporal periodicity of PT.

Proof. The periodic input $\mathcal{I}$ under consideration presents one presynaptic spike for each presynaptic neuron, with periodicity T, i.e. according to (24) $t_{j+1}^{pre} - t_j^{pre} = T$ (the second index is omitted because it is identical for all neurons). Let us consider the interval between two generic postsynaptic spikes $[t_h^{post}, t_{h+1}^{post})$, where again, the neuron index i is omitted because, as notice above, in memristor crossbar networks, postsynaptic neurons are uncoupled.

We assume that the last presynaptic spike prior to the postsynaptic spike t_h^{post} occurs for the presynaptic neuron of order J and that P presynaptic-spikes occur in $[t_h^{post}, t_{h+1}^{post})$. According to (19), by neglecting the effect of the programming pulse, the voltage $u(t)$, due to the input $\mathcal{I}$, in the generic interval $[t_h^{post}, t_{h+1}^{post})$ can be written as follows:

$$\begin{aligned} u(t) &= R \sum_{p=1}^{P} \hat{\mathbf{G}}_{J+p}(t_{J+p}^{pre})\, v_{J+p}^{pre}(t) \\ v_{J+p}^{pre}(t) &= V_H \left[\epsilon(t - t_{sh} - t_{j,k}^{pre}) - \epsilon(t - t_{sh} - t_H - t_{j,k}^{pre})\right] \end{aligned} \quad (30)$$

As already noticed, the threshold u^{th} can only be reached during a presynaptic heating pulse. Without losing generality, as illustrated in Fig. (13), we may assume that the threshold, giving rise to the postsynaptic spike t_h^{post} occurs after a time αt_H from the beginning of the J^{th} presynaptic heating pulse.

By assuming that the voltage $u(t)$ is reset after the postsynaptic spike, the above expression (30) takes the form:

$$\begin{aligned} u(t) &= RV_H \sum_{p=1}^{P} \hat{\mathbf{G}}_{J+p}(t_{J+p}^{pre}) \left[\epsilon(t - t_h^{post} - pT + \alpha t_H) \right. \\ &\quad \left. - \epsilon(t - t_h^{post} - pT + \alpha t_H - t_H)\right] \end{aligned} \quad (31)$$

To simplify (31) we note that the index J, which indicates the order of the presynaptic spike, preceding the t_h^{post} postsynaptic spike, can be omitted. In addition we observe that if we denote by $\hat{\mathbf{G}}_p^0$ the mem-conductance values in correspondence of the occurrence of the t_h^{post} postsynaptic spike, then, according to (20) and (26), $\hat{\mathbf{G}}_p(t_p^{pre})$ is given by $\hat{\mathbf{G}}_p^{1/2}$, i.e. it is obtained by $\hat{\mathbf{G}}_p^0$ through a post/pre variation.

By employing the above simplified notation, the following expression for the voltage $u(t)$ at $t = t_h^{post} + PT$ is easily derived from (31):

$$\begin{aligned} u(t_h^{post} + PT) = RV_H &\left\{ \sum_{p=1}^{P-1} \hat{\mathbf{G}}_p^{1/2} \exp\left(-\frac{(P-p)T}{\tau_m}\right) \right. \\ &\cdot \left[\exp\left(-\frac{(\alpha-1)t_H}{\tau_m}\right) - \exp\left(-\frac{\alpha t_H}{\tau_m}\right)\right] \\ &\left. + \hat{\mathbf{G}}_P^{1/2} \left[1 - \exp\left(-\frac{\alpha t_H}{\tau_m}\right)\right] \right\} \end{aligned} \quad (32)$$

Similarly, the postsynaptic voltages occurring at the end of the heating pulses of the first $P-1$ presynaptic spikes, can be derived from (31) as $u_q = u[t_h^{post} + qT + (1-\alpha)t_H]$, $(1 \leq q \leq P-1)$:

This article has been accepted for publication in IEEE Transactions on Circuits and Systems--I: Regular Papers. This is the author's version which has not been fully edited and content may change prior to final publication. Citation information: DOI 10.1109/TCSI.2021.3137713

$$u_q = u[t_h^{post} + qT + (1-\alpha)t_H] = RV_H \left\{ \sum_{p=1}^{q} \hat{\mathbf{G}}_p^{1/2} \cdot \exp\left(-\frac{(q-p)T}{\tau_m}\right)\left[1-\exp\left(-\frac{t_H}{\tau_m}\right)\right]\right\} \quad (33)$$

The following considerations hold:

1) If the set of P equations (26)-(27) is satisfied, each mem-conductance $\hat{\mathbf{G}}_p^0$, $(1 \le p \le P)$ turns out to be unaltered after a pre/post/pre triplet.
2) The second side of (32) is identical to the second side of (28), which means that if the additional $P+1$ equation (28) is satisfied, then the voltage threshold u^{th} is reached at $t = t_h^{post} + PT$. It follows that PT is the time interval between the two subsequent postsynaptic spikes under consideration t_h^{post} and t_{h+1}^{post}, i.e. $t_{h+1}^{post} - t_h^{post} = PT$.
3) It is readily verified that the voltages u_q given by (33) satisfy the following property:

$$u_q \le u_{q+1}, \quad (1 \le q \le P-2) \quad (34)$$

which implies that the maximum value of u_q is u_{P-1}. Since the maximum of $u(t)$ is reached in correspondence of the end of the heating pulse of a presynaptic spike, u_{P-1} also represents the maximum value taken by $u(t)$ as a result of the contribution of the first $P-1$ presynaptic spikes. It is readily observed that the expression of u_{P-1}, i.e. (33) with $q = P-1$, is identical to the first side of inequality (29). Hence if (29) is satisfied the voltage $u(t)$ remains below the threshold u^{th} until the end of the heating pulse of the $P-1^{th}$ presynaptic spike, which implies, according to (32) that the threshold is reached for the first time at $t = t_{h+1}^{post} = t_h^{post} + PT$.

Let us now consider a pattern composed by a replica of P mem-conductances $\hat{\mathbf{G}}_1^0, \hat{\mathbf{G}}_2^0, \cdots, \hat{\mathbf{G}}_P^0$ satisfying (25) - (28), and (29). It is readily seen that such a pattern is an equilibrium point of the discrete-time dynamic system described by (20) - (22), which proves the first part of the thesis, i.e. the existence of a steady state solution with spatial periodicity P. Moreover, since for such a pattern $t_{h+1}^{post} - t_h^{post} = PT$, it is also proved that postsynaptic spikes occurs with a periodicity of PT, which is the second part of the thesis. ■

It is worth noting that by studying the curves representing $\Delta^{pre/post/pre}(\hat{\mathbf{G}}_p, \gamma_p^{post/pre}, \gamma_p^{pre/post})$ as a function of $\hat{\mathbf{G}}_p$, it is derived that either they do not exhibit zeroes (which means that the mem-conductance converges to G_{min} or G_{max}) or they presents a negative slope in correspondence of the zero, thereby implying that the solution is stable.

The above result may have some significant applications. A first application regards the study of the dynamic behavior of spiking networks, and the consequent characterization of space and temporal periodic patterns. A second application concerns the investigation of unsupervised learning mechanisms occurring in memristive networks. Extensive numerical solutions of (25) - (28) show that each presynaptic frequency is dynamically encoded onto a mem-conductance pattern. Hence

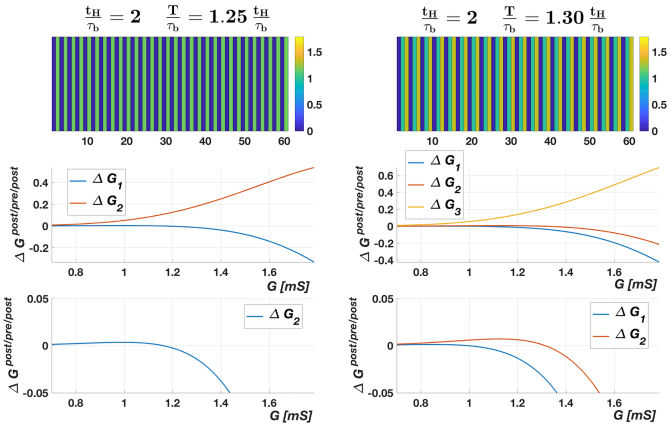

Figure 14: Spiking network composed by 60 presynaptic neurons and one postsynaptic neuron. Upper part: mem-conductance pattern periodicity (2, for $\frac{T}{\tau_b} = 1.25\frac{t_H}{\tau_b}$, and 3, for $\frac{T}{\tau_b} = 1.3\frac{t_H}{\tau_b}$); lower parts: mem-conductance variations, due to a sequence of post/pre/post spikes.

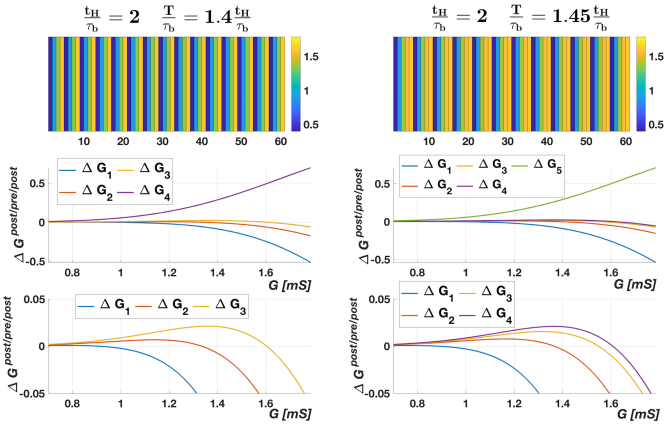

Figure 15: Spiking network composed by 60 presynaptic neurons and one postsynaptic neuron. Upper part: mem-conductance pattern periodicity (4, for $\frac{T}{\tau_b} = 1.4\frac{t_H}{\tau_b}$, and 5, for $\frac{T}{\tau_b} = 1.45\frac{t_H}{\tau_b}$); lower parts: mem-conductance variations, due to a sequence of post/pre/post spikes.

such patterns can be exploited for classifying different sets of presynaptic spikes. Finally, a third application regards the possibility of developing supervised learning techniques to optimize network performance. As shown in [29], this would require estimating the mem-conductance pattern, which maximizes the probability of a given postsynaptic output. We expect that also this task could be effectively addressed by further elaborating our dynamic system-based approach.

As an example, we have examined a network of 60 presynaptic neurons. The results are shown in Fig. 14 and 15 for $t_H = 2\tau_b$ and increasing values of the input period, i.e. decreasing values of the input frequency. The following observations hold: 1) as expected, the mem-conductance pattern and the postsynaptic spike periodicity increase with the presynaptic periodic input T, ranging from a spatial periodicity of 2 (with temporal period $2T$) for presynaptic period $\frac{T}{\tau_b} = 1.25\frac{t_H}{\tau_b}$ to a spatial periodicity of 5 (with temporal

This article has been accepted for publication in IEEE Transactions on Circuits and Systems--I: Regular Papers. This is the author's version which has not been fully edited and content may change prior to final publication. Citation information: DOI 10.1109/TCSI.2021.3137713

period $5T$) for $\frac{T}{\tau_b} = 1.45\frac{t_H}{\tau_b}$; 2) the first $P-1$ mem-conductances converge to a stable value comprised in the range (G_{min}, G_{max}), characterized by a zero of the post-pre-post curve, with a negative slope; 3) the P^{th} mem-conductance assumes the value G_{max}, in accordance with (26), because the post-pre-post variation is always positive for any $\hat{\mathbf{G}}$ in the interval (G_{min}, G_{max}); 4) the network simulation, obtained by applying 240 iterations of each input sequence, reproduces precisely the results theoretically predicted by (25) - (28). As a final remark, we note that the results also provide a theoretical framework for understanding temporal learning properties of second order memristors [15], [14].

VII. Conclusion

In this manuscript we have firstly derived a simplified analytical model of second order memristors, which only involves two variables, the mem-conductance and the internal temperature, directly attributable to the quantities used in some advanced biophysical models, namely the synaptic efficacy and the calcium concentration. Then, by exploiting this model, which allows computing the mem-conductance variation for multiple combinations of spike inputs, we have investigated the synaptic properties of single memristors and the global dynamics of memristor spiking networks. For what concerns the memristor behavior as a synapse, we have examined in detail the response to some relevant stimulation protocols, in particular cycles of spike pairs, triplets, and quadruplets at different frequencies. Through our approach, we have shown that: I) the most significant synaptic properties of second-order memristors can be easily studied and predicted; II) a significant portion of the synaptic behaviors that are not captured by classical spike pair based STDP models can be readily reproduced. As far as memristor networks are concerned, they have been accurately characterized as discrete nonlinear dynamic systems, with mem-conductances as state variables and pre and postsynaptic spikes as inputs and outputs. We have explicitly derived the state equations governing the mem-conductance evolution, and we have proved that the network response to periodic presynaptic inputs can be readily determined by computing the system equilibrium points and discussing their stability properties. We are confident that by employing together our second-order model and some theoretical and numerical advanced nonlinear dynamic techniques, the response of memristor networks to arbitrary presynaptic inputs and the underlying learning mechanisms can be further effectively investigated.

Appendix A

In this appendix, we show that the second order memristor model developed in sections II and III and particularly the mem-conductance expressions (9) - (10) derived in section III are accurate for the whole voltage range of interest and for any admissible activation Energy E_a.

We first note that the exact current-voltage characteristic (1) of the second-order memristor explicitly depends only on the two geometric parameters $\mathbf{g}$ and $\mathbf{r}$. However, it implicitly depends on the activation energy E_a since both the gap length $\mathbf{g}$, and the radius $\mathbf{r}$ are related to E_a through differential equations (2)-(3), and (4).

It is shown in Figs. 3-4 that the mem–conductance exhibits a weak dependence on the gap length g for reasonably small values of g ($0 \leq \mathbf{g} \leq 0.4\,nm$ for voltages below $1V$, and $0 \leq \mathbf{g} \leq 0.8\,nm$ for voltages between 1 and 2 V). Furthermore by increasing the voltage above $2V$ the weak dependence range extends beyond $0.8\,nm$.

Since the mem-conductance expressions (9) and (10) fully incorporates the radius dependence, to prove their accuracy, it is sufficient to show that the variation range of $\mathbf{g}$ lies within

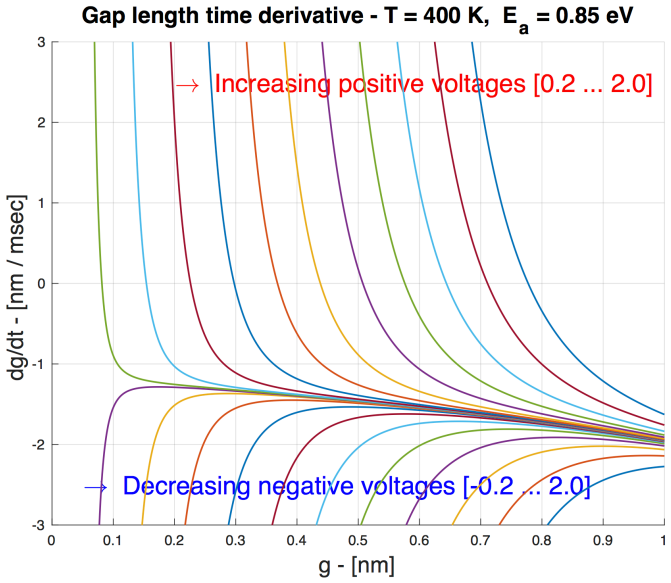

Figure 16: Gap length time derivative $d\mathbf{g}/dt$ as a function of $\mathbf{g}$, for $T = 400\,K$, $\mathbf{r}/r_0 = 1$, $E_a = 0.85\,eV$ and different input voltages ranging from $-2\,V$ to $2\,V$.

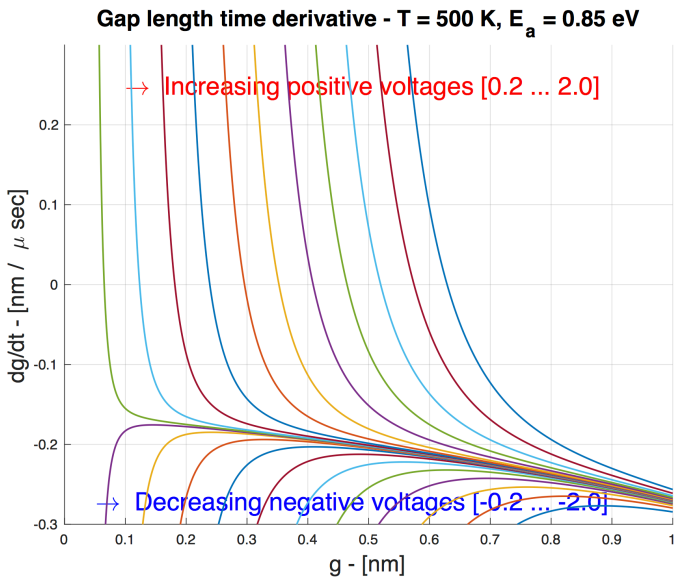

Figure 17: Gap length time derivative $d\mathbf{g}/dt$ as a function of $\mathbf{g}$, for $T = 500\,K$, $\mathbf{r}/r_0 = 1$, $E_a = 0.85\,eV$ and different input voltages ranging from $-2\,V$ to $2\,V$.

This article has been accepted for publication in IEEE Transactions on Circuits and Systems--I: Regular Papers. This is the author's version which has not been fully edited and content may change prior to final publication. Citation information: DOI 10.1109/TCSI.2021.3137713

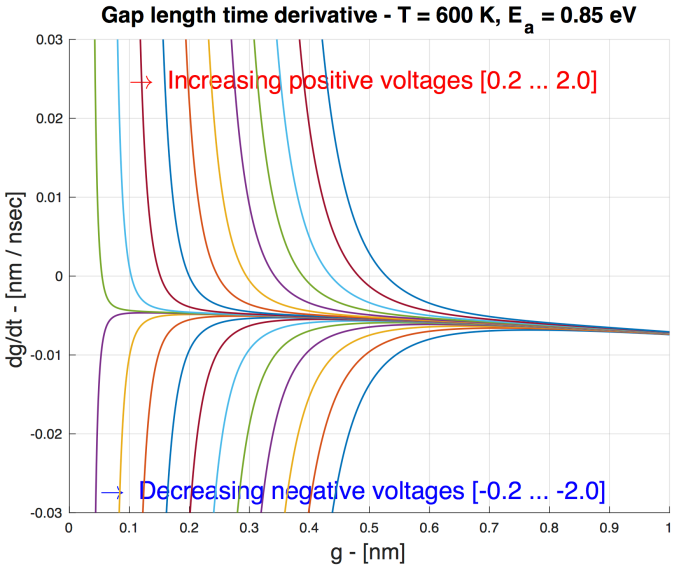

Figure 18: Gap length time derivative $d\mathbf{g}/dt$ as a function of $\mathbf{g}$, for $T = 600\,K$, $\mathbf{r}/r_0 = 1$, $E_a = 0.85\,eV$ and different input voltages ranging from $-2\,V$ to $2\,V$.

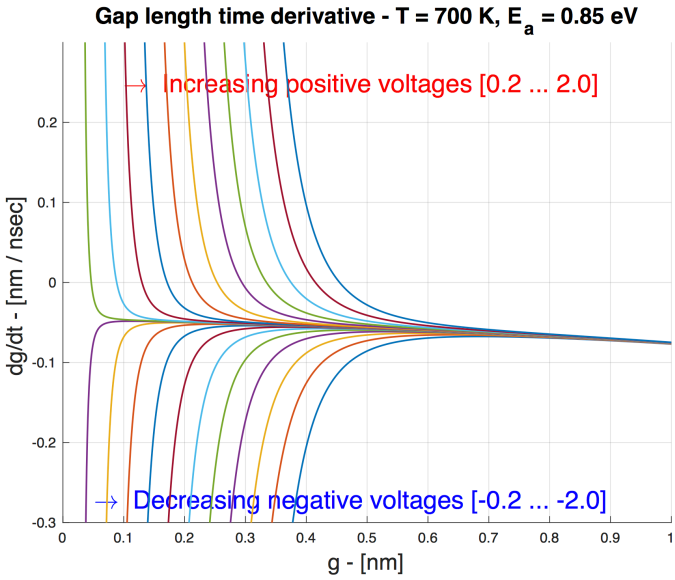

Figure 19: Gap length time derivative $d\mathbf{g}/dt$ as a function of $\mathbf{g}$, for $T = 700\,K$, $\mathbf{r}/r_0 = 1$, $E_a = 0.85\,eV$ and different input voltages ranging from $-2\,V$ to $2\,V$.

the interval $[0, 0.8nm]$. By examining equation (2) - (3) it is noticed that, for constant voltages, the zeroes of the the gap length time derivative $d\mathbf{g}/dt$ are given by the solutions of eq. (3), which does not depend on the activation energy:

$$\frac{\alpha\, a^2\, f}{\mathcal{L}_0 - \mathbf{g}} - 2\, a\, f \sinh\left(\frac{q\, a\, \mathbf{v}}{\mathbf{g}\, k_b\, \mathbf{T}}\right) = 0 \tag{35}$$

The graph of the gap-length time derivative $d\mathbf{g}/dt$ as a function of $\mathbf{g}$ is shown in Figs. 16-19, for $E_a = 0.85\,eV$, different values of the temperature, within the interval reached during the heating phase, and constant voltages ranging from -2 to 2 V.

For negative voltages the time derivative is always negative and therefore we may assume that the gap length remains below the values reached with positive inputs.

For positive voltages, each curve exhibits a single zero, which depends on the voltage and on the temperature. By denoting with $\hat{\mathbf{g}}(\mathbf{v}, \mathbf{T})$ such zeroes, due to the negative slope, it is expected that the gap length $\mathbf{g}(t)$ lies in the interval $[0, \hat{\mathbf{g}}(\mathbf{v}, \mathbf{T})]$, i.e. $\hat{\mathbf{g}}(\mathbf{v}, \mathbf{T})$ can be considered the greatest value assumed by the gap length for given voltages and temperatures.

It is observed from Figs. 16-19 that: a) for positive voltages the zeroes $\hat{\mathbf{g}}(\mathbf{v}, \mathbf{T})$ decreases as the temperature increases; b) for given temperatures the zeroes $\hat{g}(\mathbf{v}, \mathbf{T})$ increases as the voltage increases.

In the temperature range under consideration, from 400 to $700\,K$, the greatest value of $\hat{\mathbf{g}}(\mathbf{v}, \mathbf{T})$, reached for $T = 400\,K$ and $\mathbf{v} = 2\,V$, is less than $0.8\,nm$; for voltages inferior to $1V$ the greatest value is below $0.4nm$. According to Figs. 3-4 it turns out that in both cases ($0 \leq \mathbf{v} \leq 1$ and $\mathbf{g}(t) < 0.4\,nm$, $1 \leq \mathbf{v} \leq 2$ and $\mathbf{g}(t) < 0.8\,nm$) the mem–conductance presents a weak dependence on the gap length and therefore its approximate expression is accurate for $E_a = 0.85\,eV$. Note that for higher voltages, superior to $2V$, the time derivative zeroes slightly shift beyond $0.8nm$, but the gap length range for which the mem.-conductance substantially depends on the sole radius $\mathbf{r}$ also increases.

As noticed above, if different activation energy values are considered, the zeroes of the gap length time derivative $d\mathbf{g}/dt$ are not altered, and the graph of $d\mathbf{g}/dt$ versus $\mathbf{g}$ is accordingly obtained by a suitable scaling on the vertical axis. Since the zeroes $\hat{g}(\mathbf{v}, \mathbf{T})$ are not changed, we may conclude that the mem-conductance approximation holds for the actual input voltage ranges and for each admissible value of the activation energy E_a.

The above analysis also shows that the model is pretty accurate for any gap length in the interval $[0, 0.8\,nm]$, and hence also works in the absence of gap.

Appendix B

In this Appendix, we examine the effect of parameter variations on the proposed second order memristor model. It is shown in Appendix A that the mem-conductance presents a weak dependence on the gap-length within the range of interest. The mem-conductance expression (10), on which the second order model is based, fully includes the dependence on the radius r and the related parameters r_0 and r_m. In order to evaluate the effect of the device intrinsic parametric variations, it is worth examining the dependence of the STDP function on the parameters r_0 and r_m.

The STDP function is derived from the mem-conductance time derivative (12), which is expressed as the product of two terms, the first containing the temperature and the second, $\eta(\hat{\mathbf{G}})$, depending on r_0 and r_m.

The sensitivity of the mem-conductance time derivative with respect to the parameter variation is therefore equivalent to the

This article has been accepted for publication in IEEE Transactions on Circuits and Systems--I: Regular Papers. This is the author's version which has not been fully edited and content may change prior to final publication. Citation information: DOI 10.1109/TCSI.2021.3137713

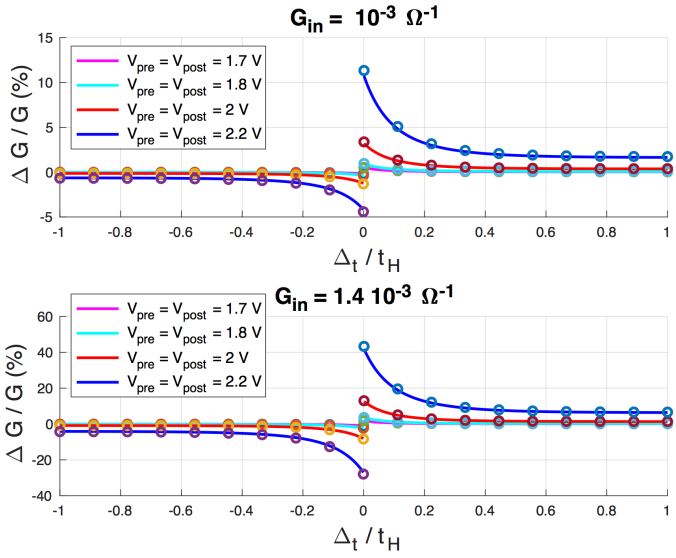

Figure 20: Impact on STDP functions of a 5 % variation of the parameter r_0. A continuous line represents nominal values, circles represent perturbed values.

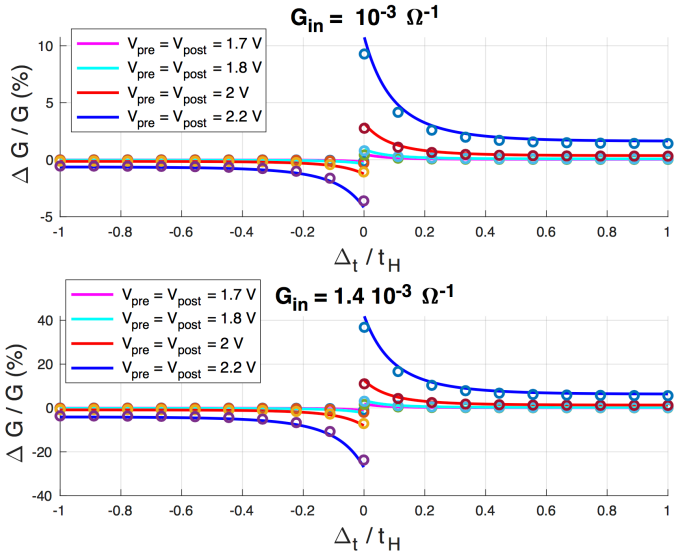

Figure 21: Impact on STDP functions of a 5 % variation of the parameter r_m. A continuous line represents nominal values, circles represent perturbed values.

sensitivity of $\eta(\hat{\mathbf{G}})$, that can be readily derived from (13):

$$\frac{r_0}{\eta(\hat{\mathbf{G}}, r_0)} \frac{\partial \eta(\hat{\mathbf{G}}, r_0)}{\partial r_0} = \frac{\frac{r_m}{r_0} - 2\sqrt{\frac{R_s\hat{\mathbf{G}}}{1-R_s\hat{\mathbf{G}}}}}{\sqrt{\frac{R_s\hat{\mathbf{G}}}{1-R_s\hat{\mathbf{G}}}} - \frac{r_m}{r_0}} \tag{36}$$

$$\frac{r_m}{\eta(\hat{\mathbf{G}}, r_m)} \frac{\partial \eta(\hat{\mathbf{G}}, r_m)}{\partial r_m} = \frac{\frac{r_m}{r_0}}{\sqrt{\frac{R_s\hat{\mathbf{G}}}{1-R_s\hat{\mathbf{G}}}} - \frac{r_m}{r_0}} \tag{37}$$

From Eqs. (36) and (37) it is seen that the sensitivity only depends on the mem-conductance $\hat{\mathbf{G}}$ and on the nominal values of the parameters r_0 and r_m. As a consequence for a small perturbation of the parameters, the STDP variation is only affected by the mem-conductance value and not by the time shift Δ_t between pre/post (post/pre) pairs.

Figs. 20-21 show some examples, from which it is seen that STDP curves are only marginally affected by small variations of the parameters r_0 and r_m. Extensive simulations have confirmed that the proposed simplified model is sufficiently robust to accurately described the main second order memristor functionalities, in presence of intrinsic device parameter variations.

REFERENCES

[1] L. O. Chua, "Memristor - The missing circuit element," *IEEE Transactions on Circuit Theory* . vol. 18, no. 5, pp. 507–519, 1971.

[2] L. O. Chua and S. M. Kang, 'Memristive devices and systems," *Proceedings of the IEEE*, vol. 64, no. 2, pp. 209–223, 1976.

[3] D. B. Strukov, G. S. Snider, D. R. Stewart, and R. S. Williams, "The missing memristor found," *Nature*, vol. 453, no. 7191, pp. 80–83, 2008.

[4] S. Shin, K. Kim, and S. M. Kang, "Memristor applications for programmable analog ICs," *IEEE Transactions on Nanotechnology*, vol. 10, no, 2, pp. 266-274, 2010.

[5] J. Borghetti, G. S. Snider, P. J. Kuekes, J. J. Yang, R. Duncan, and R. S. Williams, "Memristive'switches enable 'stateful'logic operations via material implication," *Nature*, vol. 464, pp. 873-876, 2010.

[6] H. Bao, Z. Hua, H. Li, M. Chen, and B. Bao, "Discrete Memristor Hyperchaotic Maps," *IEEE Transactions on Circuits and Systems I: Regular Papers*, pp. 1-11, 2021.

[7] S. H. Jo, T. Chang, I. Ebong, B. B. Bhadviya, P. Mazumder, and W. Lu, "Nanoscale memristor device as synapse in neuromorphic systems," *Nano Letters*, vol. 10, no. 4, pp. 1297–1301, 2010.

[8] S. Kim, C. Du, P. Sheridan, W. Ma, S. Jin Choi, and W. D. Lu, "Experimental demonstration of a second-order memristor and its ability to biorealistically implement synaptic plasticity," *Nano Letters*, vol. 15, pp. 2203-2211, 2015.

[9] S. Kim, H. D. Kim, and S. J. Choi, "Compact two-state-variable second-order memristor model," *Small (Weinheim an der Bergstrasse, Germany)*, vol. 12, no. 5, 2016.

[10] R. Yang, H. M. Huang, Q. H. Hong, X. B. Yin, Z. H. Tan, T. Shi, Y. X. Zhou, X. S. Miao, X. P. Wang, S. B. Mi, C. L. Jia, and X. Guo, "Synaptic suppression triplet-STDP learning rule realized in second-order memristors," *Advanced Function Material*, vol. 28, pp. 1-10, 2018.

[11] A. Ascoli, F. Corinto, V. Senger and R. Tetzlaff, "Memristor Model Comparison," *IEEE Circuits and Systems Magazine*, vol. 13, no. 2, pp. 89-105, 2013.

[12] Q. Xia, J. J. Yang, "Memristive crossbar arrays for brain-inspired computing," *Nature Materials*, vol. 18, pp. 309–323, 2019.

[13] Y. Zhang, Z. Wang, J. Zhu, Y. Yang, M. Rao, W. Song, Y. Zhuo, X. Zhang, M. Cui, L. Shen, R. Huang, J. J. Yang, "Brain-inspired computing with memristors: Challenges in devices, circuits, and systems," *Applied Physics Reviews*, 7, 2020.

[14] M. A Zidan, Y. Leong and W. D. Lu, "Temporal learning using second order memristors," *IEEE Transactions on Nanotechnologies*, vol. 16, no. 4, pp. 721–723, 2017.

[15] Y. Jeong and W. D. Lu, "Neuromorphic computing using memristor crossbar networks," *IEEE Nanotechnologies Magazine*, pp. 6–18, September 2018.

[16] H. Markram, J. Lubke, M. Frotscher, and B. Sackmann, "Regulation of synaptic efficacy by coincidence of postsynaptic," *Science*, vol. 275, no 5297, pp. 213-215, 1997.

[17] G. Bi and M. Poo, "Synaptic modifications in cultured hyppocampal neurons: dependence on spike timing, synaptic strength, and postsynaptic cell type," Regulation of synaptic efficacy by coincidence of postsynaptic," *Journal of Neuroscience*, vol. 18, no. 24, pp. 10464-10472, 1998.

[18] P. J Sjostrom, G. G. Turrigiano, and S. B. Nelson, "Rate, timing and cooperativity jointly determine cortical synaptic plasticity," *Neuron*, vol. 3, pp. 1149-1164, 2001.

[19] G. Bi and M. Poo, "Synaptic modifications by correlated activity: Hebb's potential revisited," *Annu. Rev. Neuroscience*, vol. 24, pp. 139-166, 2001.

[20] P. J Sjostrom, E. A. Rankz, A. Roth, and M. Hausser, "Dendritic excitability and synaptic plasticity," *Physiol. Rev.*, vol. 88, pp. 769-840, 2008.

[21] R. C Malenka, J. Kauer, R. Zucker, and R. A Nicoll, "Post synaptic calcium is sufficient for potentiation of hippocampal synaptic transmission," *Science*, vol. 242, pp. 81-84, 1997.

[22] J Lisman, "A mechanism for hebb and hebb-processes underlying learning and memory," *Proceedings of the National Academy of Sciences - USA*, vol. 86, pp. 9574-9578, 1989.

[23] H. Z Shouval, M. F. Bear, L. N Cooper, "A unified model of NMDA receptor dependent bidirectional synaptic plasticity," *Proceedings of the National Academy of Sciences - USA*, vol. 99, pp. 10381-10386, 2002.

[24] J Lisman and N Spruston, "Postsynaptic depolarization requirements for LTP and LTD: a critique of spice-timing-dependent plasticity," *Nature Neuroscience*, vol. 8, pp. 839-841, 2005.

[25] J. P. Pister and W. Gernster, "Triplets of spikes in a model of spike-timing-dependent plasticity," *Journal of Neuroscience*, vol. 26, pp. 9673-9682, 2006.

[26] M Graupner and N Brunel, "Calcium-based plasticity model explains sensitivity of synaptic changes to spike pattern, rate, and dendritic location," *Proceedings of the National Academy of Sciences - USA*, vol. 109, pp. 3991-3996, 2012.

[27] R. Kempter, W. Gernster, and J. Leo. van Hammen,"Hebbian learning and spiking neuron," *Physical Review E*, vol. 59, no. 4, pp. 4498-4514, 1999

[28] W. Mass, and H. Markram, "On the computational power of circuits of spiking neurons," *J. Comput. Syst. Sci.*, vol. 69, pp. 593-616, 2004.

[29] J. P. Pfister, T. Toyoizumi, D. Barber and W. Gernster,"Optimal spike-timing-dependent plasticity for precise action potential firing in supervised learning," *Neural Computation*, vol. 18, pp. 1318-1348, 2006.

[30] W. Senn and J. P Pfister, "Spike-timing-dependent plasticity, Learning rules, *Encyclopedia of Computational Neuroscience* Springer, New York, 2015.

[31] F. Marrone, G. Zoppo, F. Corinto, and M. Gilli, "Second order memristor models for neuromorphic computing," *IEEE International Midwest Symposium on Circuits and Systems*, 2019.

[32] F. Marrone, G. Zoppo, F. Corinto, and M. Gilli, "Pattern Characterization in Second Order Memristor Network," *IEEE International Midwest Symposium on Circuits and Systems*, 2020.

[33] F. Marrone, G. Zoppo, F. Corinto, and M. Gilli, "A Dynamic System Approach to Spiking Memristor Network Investigation," *Late Breaking News - IEEE International Midwest Symposium on Circuits and Systems*, 2021.

Francesco Marrone (Member, IEEE) received the B.Sc. and M.Sc. degrees in electronics engineering from the Politecnico di Torino, Italy, in 2015 and 2018, respectively, where he is currently pursuing the Ph.D. degree with the Department of Electronics and Telecommunication. His research interests include nonlinear dynamics, neuromorphic computing, and memristive technologies.

Gianluca Zoppo received the B.Sc. degree in mathematics and the M.Sc. degree in stochastics and data science from the Università di Torino, Italy, in 2016 and 2018, respectively, where he is currently pursuing the Ph.D. degree with the Department of Electronics and Telecommunication. His research interests include nonlinear dynamics, neuromorphic computing, and MCMC optimization.

Fernando Corinto (Senior Member) received the Masters' Degree in Electronic Engineering and the Ph.D. degree in Electronics and Communications Engineering from the Politecnico di Torino, in 2001 and 2005 respectively. He also received the European Doctorate from the Politecnico di Torino, in 2005. F. Corinto was awarded a Marie Curie Fellowship in 2004. Fernando Corinto is currently a Professor of Electrical Engineering with the Department of Electronics and Telecommunications, Politecnico di Torino. His research activities are mainly on nonlinear circuits and systems, locally coupled nonlinear/nanoscale networks, and memristor nanotechnology. Fernando Corinto is co-author of "Nonlinear Circuits and Systems with Memristors: Nonlinear Dynamics and Analogue Computing via the Flux-Charge Analysis Method" (published by Springer in 2021), 7 book chapters and more than 150 international journal and conference papers. Since 2010, he is Senior Member of the IEEE. He served as Chair of the IEEE CAS Technical Committee on Cellular Nanoscale Networks and Array Computing and Member of the IEEE CAS TC Nonlinear Circuits and Systems. Fernando Corinto has been Associated Editor of the IEEE Trans. on Circuits and Systems - I for 2014-2015. He is also in the Editorial Board and Review Editor of the International Journal of Circuit Theory and Applications since January 2015. Fernando Corinto was the Vice Chair of the COST Action: Memristors - Devices, Models, Circuits, Systems and Applications (MemoCiS). Prof. Corinto has been DRESDEN Senior Fellows at the Technische Universitat Dresden in 2013 and 2017. He has been August- Wilhelm Scheer visiting professor at Technische Universitat München in 2016 and he is also member of the Institute for Advanced Study -Technische Universitat Munchen.

Marco Gilli (Fellow Member) is a Professor of Electrical Engineering at the Politecnico di Torino. From May 2002 to September 2003 he was Deputy Dean of the First Faculty of Engineering at the Politecnico di Torino and from October 2003 to September 2005 he was Vice Dean of the same Faculty (responsible for the Graduate School). From October 2005 to February 2012 he served as Deputy Rector (responsible for Academic Affairs) and from February 2012 to March 2018 he served as Rector of the Politecnico di Torino.
From 2012 to 2014 he served as President of CESAER (Conference of European Schools for Advanced Engineering Education and Research).
Since July 2019 he has been serving as a Scientific Attaché at the Embassy of Italy in the USA.
His research activity is mainly in the area of nonlinear circuits and systems, cellular neural/nonlinear networks, including machine learning, nonlinear network theory and applications and partially in the field of electromagnetic theory. He is co-author of two papers that received the Best Paper Award in 1994 and 2004 from the International Journal of Circuit Theory and Applications. He is also author or co-author of more than 200 scientific publications in international journals and in the proceedings of international conferences.
Since January 2005, Marco Gilli has been a Fellow of the Institute of Electrical and Electronics Engineers (IEEE). From 1999 to 2003 he was Associate Editor of the IEEE, Transactions on Circuits and Systems. From 2006 to 2012 he served as Editor in Chief of the International Journal of Circuit Theory and Applications. Since 2010 he has been a member of the Editorial Board of the International Journal of Bifurcations and Chaos. Marco Gilli is a member of the IEEE-CAS Technical Committee on Cellular neural networks and array computing (Chair from 2007 to 2009) and of the IEEE-CAS Technical Committee on Nonlinear circuits and systems. From 2001 to 2016 he served as the Chair of the CAS Chapter of the IEEE North Italy Section and from 2005 to 2012 he was the President of the Italian Society for Chaos and Complexity. Marco Gilli has been responsible for many national and international research projects. In his capacity as Rector of the Politecnico di Torino, he was responsible for the partnership agreements with more than 40 national and international companies, including manufacturing industries (Fiat Chrysler Automobiles - FCA , General Motors - GM, General Electric/Avio Aero - GE/Avio Aero, Alenia, etc), energy industries (ENEL, ENI, TERNA, EDF, State Grid China, etc) and IT industries (ST, IBM, etc).